Lateral spreading of a near-field river plume: Observations and numerical simulations

Article · July 2009

DOI: 10.1029/2008JC004893

3 authors, including:

Daniel G Macdonald
University of Massachusetts Dartmouth
29 PUBLICATIONS **517** CITATIONS
SEE PROFILE

Robert Hetland
Texas A&M University
55 PUBLICATIONS **1,298** CITATIONS
SEE PROFILE

JOURNAL OF GEOPHYSICAL RESEARCH, VOL. 114, C07013, doi:10.1029/2008JC004893, 2009

Lateral spreading of a near-field river plume: Observations and numerical simulations

Fei Chen,[1] Daniel G. MacDonald,[1] and Robert D. Hetland[2]

Received 29 April 2008; revised 9 February 2009; accepted 5 May 2009; published 11 July 2009.

[1] Data collected from the near-field region of the Merrimack River (Massachusetts) plume were analyzed to examine plume spreading. Estimates of the plume spreading rate were derived from a direct assessment of the spreading of clustered surface drifters and from density and velocity data along a cross-plume arc. Additionally, plume spreading rates were also derived from highly resolved numerical model output (ROMS). These three distinct observational and numerical approaches have reasonable agreement and are compared favorably with observations using a control volume approach in a previous study. It is demonstrated that these three methods are valid to estimate the plume spreading rate. The observations and numerical simulations also allowed estimation of terms in the lateral momentum balance along streamline normals, perpendicular to surface layer streamlines. One principal finding of this study is that the dominant terms in the lateral momentum balance are the centrifugal force term associated with streamline curvature, the buoyancy term, the Coriolis term, and the interfacial stress term. Furthermore, the lateral momentum balance shows that the lateral spreading process is significantly affected by interfacial stress within the first 1 to 2 km but, thereafter, is locally inviscid. However, turbulent mixing continues to play an important role in modifying the spreading rate by adjusting the internal wave speed.

Citation: Chen, F., D. G. MacDonald, and R. D. Hetland (2009), Lateral spreading of a near-field river plume: Observations and numerical simulations, *J. Geophys. Res.*, *114*, C07013, doi:10.1029/2008JC004893.

1. Introduction

1.1. Spreading and Cross-Plume Momentum

[2] Buoyant surface plumes are generated in the coastal ocean by the discharge of fresh water from rivers and estuaries. These plumes are characterized by a distinct contrast in properties between plume and ambient water [*Wright and Coleman*, 1971; *Yankovsky and Chapman*, 1997]. Traditionally, studies associated with buoyant plumes have focused on the far-field [e.g., *Lentz and Largier*, 2006], where plume dynamics are dominated by buoyant effects, mixing is controlled primarily by wind stress, and the effects of the earth's rotation are important. *Horner-Devine et al.* [2009] describe the transition of a plume from discharge to the far field through a series of progressively less energetic regions, each representing a distinct timescale associated with plume evolution. Recent calculations and observations have suggested that mixing in the relatively small near-field region of a plume may be on the same order as mixing in the far-field [e.g., *Hetland*, 2009]. Thus the near-field region may play an important, although originally overlooked, role in coastal dynamics. The near-field region of a buoyant plume can be defined as the region where momentum dominates over buoyancy and the plume acts like a buoyant jet [*Jirka et al.*, 1981]. In the near-field region, an initial momentum anomaly enhances velocity shear and initiates turbulent mixing, while a strong density difference between the plume and ambient water limits shear induced mixing and causes lateral gravitational spreading of the buoyant water, resulting in a shoaling of the upper layer [*Luketina and Imberger*, 1987; *Hetland*, 2005]. Linkages between spreading and shoaling of the plume, and interfacial mixing, make it critically important to understand the dynamics of spreading in the near field in order to properly characterize the local mixing environment, and understand the implications for the larger coastal ocean.

[3] The evolution of plume structure in the near-field region has been addressed in both the engineering and oceanographic literature [e.g., *Adams and Stolzenbach*, 1977; *MacDonald and Geyer*, 2004; *Hetland and MacDonald*, 2008]. When a buoyant outflow is discharged onto a sloping bottom, the well-mixed jet is initially bottom attached, until hydraulic conditions force a lift-off, and detachment from the bottom [*MacDonald and Geyer*, 2005]. This often occurs at some bathymetric transition, such as a sill, or change in bottom slope. Some recent studies on turbulence and mixing in near-field plumes suggest that mixing can play an important role in near-field plume dynamics [e.g., *MacDonald et al.*, 2007; *Chen and MacDonald*, 2006; *McCabe et al.*, 2008], by significantly increasing stress, and converting kinetic energy to potential energy.

[1]Department of Estuarine and Ocean Sciences, School for Marine Science and Technology, University of Massachusetts Dartmouth, Fairhaven, Massachusetts, USA.
[2]Department of Oceanography, Texas A&M University, College Station, Texas, USA.

0148-0227/09/2008JC004893$09.00

[4] It is important to understand plume spreading in the near-field region because of the complicated but poorly understood relationship between lateral spreading and mixing of the plume with ambient waters [e.g., *Hetland*, 2009]. For example, mixing of the buoyant outflow and the dense ambient water in the lower layer reduces the momentum and density anomaly between the two layers [*Garvine*, 1984; *MacDonald and Geyer*, 2004], thereby affecting the spreading rate, which depends on the density difference between the plume and ambient waters. Mixing occurring in the near-field is important because it has the same order as the mixing in the far-field. Moreover, as pointed out by previous studies [e.g., *MacDonald et al.*, 2007; *Hetland*, 2009], mixing and spreading are related. In order to fully understand the mechanisms for mixing, we need to understand spreading in the near-field at the same time.

[5] It has been suggested that the lateral spreading of buoyant plumes should behave like a propagating lock exchange (e.g., J. B. Schijf and J. C. Schonfeld, Theoretical considerations on the motion of salt and fresh water, paper presented at Minnesota International Hydraulics Convention, Minneapolis, Minnesota, 1953), with which the spreading rate is proportional to local gravity wave speed. This has been demonstrated recently by *Hetland and MacDonald* [2008], who used numerical simulations to show that for a river plume which separates from the coastline, the plume width is proportional to radial distance from the mouth, and the local plume spreading rate is related to the local internal gravity wave speed.

[6] Many recent studies of plume spreading have been conducted with numerical models, which have proven to be a useful tool for the estimation of plume spreading rates and understanding plume structure [e.g., *O'Donnell*, 1988; *Hetland and MacDonald*, 2008]. Observational studies, incorporating traditional hydrographic survey instrumentation, such as conductivity temperature depth (CTD) probes and acoustic Doppler current profilers (ADCPs) have also been essential in providing direct observation of plume spreading, and furthering understanding of buoyant surface plumes in coastal waters [e.g., *Garvine*, 1984]. Additionally, the recent advent of low-cost, easy-to-deploy surface drifters equipped with GPS tracking devices and radio frequency, cell phone, or satellite communications have provided oceanographers with an additional tool to measure and study the upper layer currents within estuaries and the coastal ocean [*Brugge*, 1995; *Austin and Atkinson*, 2004]. These Lagrangian drifters can provide direct measurements of the surface circulation.

[7] Measurements of density and velocity structure within the plume can also allow for the estimation of terms in the lateral momentum balance [e.g., *Lentz et al.*, 2003]. *Hench and Luettich* [2003] analyzed the transient momentum balance in a streamwise coordinate to examine depth-averaged tidal flow at shallow inlets. *Geyer* [1993] discussed the tidal flow around a headland and suggested the lateral momentum equation in a streamwise coordinate system can be written as

$$\underset{(I)}{\frac{\partial u_n}{\partial t}} + \underset{(II)}{u_s \frac{\partial u_n}{\partial s}} - \underset{(III)}{\frac{u_s^2}{R_s}} + \underset{(IV)}{f u_s} + \underset{(V)}{g \frac{\partial \eta}{\partial n}} - \underset{(VI)}{\frac{\partial}{\partial z}\left(A \frac{\partial u_n}{\partial z}\right)} = 0 \quad (1)$$

where s is oriented everywhere in the direction of the flow and n is oriented orthogonal to the flow, u represents velocity, R_s is the local radius of the streamline curvature, f is the Coriolis parameter, g is the acceleration of gravity, η is the water level, and A is eddy viscosity. equation (1) indicates that in the streamline-normal direction, the terms in the momentum balance are an acceleration term (I), an advection term (II), the streamline curvature term (III), Coriolis forcing term (IV), barotropic forcing term (V), and a stress term (VI).

[8] Applying equation (1) to a steady state, two-layer, near-field plume system, in which the equation for the lower layer has been subtracted from that of the upper layer (following *Geyer* [1993]), thus removing the unknown barotropic term, yields:

$$\frac{u_{s1}^2}{R_s} - \frac{u_{s2}^2}{R_s} - u_{s1}\frac{\partial u_{n1}}{\partial s} + u_{s2}\frac{\partial u_{n2}}{\partial s} - f u_{s1} + f u_{s2} = -g'\frac{\partial h_i}{\partial n} - \frac{\tau_b}{\rho h_2} + \frac{\tau_i}{\rho}\left(\frac{h_1 + h_2}{h_1 h_2}\right) \quad (2)$$

where the subscripts 1 and 2 refer to the upper layer and the lower layer, respectively, R_s is the radius of curvature of the upper layer streamlines (clockwise positive), $g' = g(\Delta\rho)\rho_0^{-1}$ is a reduced gravity based on the density difference between the upper and lower layers, and h_i represents the height of the layer interface above an arbitrary datum. For the two-layer streamwise coordinate system, the s direction, which is the streamline direction, is defined by the local mean flow direction in upper layer, and stream-normal direction is defined positively left of the upper flow. Therefore by definition, the streamwise velocity u_s is the local flow velocity, and the vertical average normal flow in upper layer, u_{n1}, is zero everywhere in this frame of reference. Note, however, that u_n is locally nonzero, thereby giving rise to a nonzero shear ($\partial u_n/\partial z$), and the potential importance of the interfacial stress term. For the terms in equation (2), since the lower layer is almost motionless, all the terms associated with the lower layer can be considered negligible compared to those in the upper layer. The bottom stress term $\frac{\tau_b}{\rho h_2}$ is not significant because the bottom is relatively deep, compared to the interfacial depth. These approximations suggest that equation (2) can be simplified as:

$$\frac{u_{s1}^2}{R_s} - f u_{s1} = -g'\frac{\partial h_i}{\partial n} + \frac{\tau_i}{\rho}\left(\frac{h_1 + h_2}{h_1 h_2}\right) \quad (3)$$

This simplified momentum equation suggests that for a two-layer system, the curvature term, the Coriolis term, the pressure gradient due to interface slope (the "buoyancy" term) and the interfacial stress term are the dominant terms in the near-field region under steady state conditions. This simplified equation will be tested by numerical model output, and then used to examine the lateral momentum balance in the near-field plume area in the following sections.

1.2. Recent-Related Studies

[9] This study follows two recently published studies also relating to the dynamics of the near-field Merrimack River plume: *MacDonald et al.* [2007] and *Hetland and MacDonald* [2008]. In *MacDonald et al.* [2007], turbulent dissipation rates in the Merrimack River plume were estimated using a control volume approach and numerical simulation. The control volume approach was used [e.g., *MacDonald and Geyer*, 2004; *Chen and MacDonald*, 2006]

to obtain the buoyancy flux term B in the steady state turbulent kinetic energy equation. For the Merrimack River plume, the near-field region was demonstrated to be in a quasi-steady state during the mid to late ebb, as shown by the relative consistency of turbulence profiles in their Figure 10, and a limited effect of time-dependent assumptions on the size of error bars in their analysis. Turbulent dissipation rates and the structure of the turbulent field, derived from a numerical simulation using the Regional Ocean Modeling System (ROMS) were found to compare well with the control volume results.

[10] In addition to estimating turbulent quantities, *MacDonald et al.* [2007] estimated plume expansion through the conservation of freshwater flux along a transect, which was a critical component of implementing the control volume approach. The plume expansion results from this approach are used in this study as a starting point for further investigation of plume spreading through a variety of other estimation techniques.

[11] *Hetland and MacDonald* [2008] investigated plume spreading in the near-field region using a numerical simulation. Following the demonstration of a quasi-steady state during mid to late ebb, the river discharge was modeled by a steady outflow, representative of both the river discharge and the tidal flow. Such an approximation is consistent with timescales of 1–2 hours for propagation of plume water through the near-field region. The steady state assumption was also evaluated by running the model with tides, indicating that spreading rates are constant from late ebb to early flood.

[12] *Hetland and MacDonald* [2008] defined the core of the near-field plume between $-50°$ and $15°$ from due east of the river mouth (positive counterclockwise), in order to isolate the homogeneous core of the river outflow from the ambient coastal water. Their results indicate that the properties of the plume within this core, including surface salinity, turbulent dissipation rates, surface velocity and spreading rates, are all approximately functions only of the radial distance from the river mouth, and are laterally homogenous along a particular arc. Local spreading rates (δ) within the plume core were estimated using a principle strain rate approach, and compared to direct evaluations using numerical drifters. It should be noted that 5000 numerical drifters were used to evaluate local spreading rates. This study also found the rate of plume spreading rate to be proportional to the local internal gravity wave speed, c: $DW/Dt = \delta W \approx 2c$, and that relative width is related to radial distance from the mouth raised to a constant exponent derived from observations, presented as $W/W_0 = r^{1/\alpha}$, where W is the plume width and r is the radial distance. Their analyses suggested a value of $\alpha \approx 0.81$ for their model run of the Merrimack River, which means the Merrimack river plume is spreading faster than a pure radial spreading plume that has the relationship of $W/W_0 = r$, a condition referred to as a divergent plume. Although the exact value of α may vary for different regions or conditions, the analytical framework should be relevant to all plumes.

[13] In this manuscript, estimates of lateral spreading rates associated with the near-field Merrimack River plume are obtained directly from surface drifters, and also from a new analysis of numerical model output, and then compared with the control volume derived estimates from *MacDonald et al.* [2007]. Moreover, the physical forces that drive plume spreading are deduced from the lateral momentum equation (3). Finally, the momentum equation is also used to derive estimates of spreading directly from cross-plume arc data. The results provide an opportunity for comparison and validation of several different observational and numerical methods, and also provide insightful information about the lateral spreading process and the relationship between lateral spreading and turbulent mixing occurring in the near-field region.

[14] This manuscript is organized as follows. In section 2, the field site, observational tools, and numerical model setup are described. Results are presented in section 3. Section 4 contains the discussion of the lateral momentum balance of the near-field plume, comparison of observations and model output, and a discussion of the relationship between plume spreading and mixing.

2. Field Experiments and Model Description

2.1. Study Site: The Merrimack River Estuary

[15] The field experiments were performed in the near-field region of the Merrimack River plume, along the north shore of Massachusetts. The Merrimack River discharges into the Gulf of Maine, approximately 6 km south of the Massachusetts-New Hampshire border (Figure 1).

[16] The freshet in the Merrimack typically occurs in spring as increased runoff is generated due to snowmelt, local rainfall activity, and a typically saturated drainage basin. This study focuses on the dynamics of the Merrimack River plume in the first several km outside the river mouth during near record flow conditions which occurred in May 2006. The high fresh water discharge resulted in highly stratified conditions and seaward flowing water at the surface through the entire tidal cycle.

[17] Under such conditions, a salt wedge estuary results, characterized by salinity differences of approximately 20 psu across only a few meters in the vertical. During the study period, the salt wedge was observed to advance landward approximately 10 km into the river channel during the flood, and was flushed back to the mouth during ebb. At this point in the tidal cycle, after the salt wedge had retreated to the mouth, there existed a period of quasi-steady state dynamics for several hours, prior to the salt wedge advancing into the channel on the next flooding tide. This paper focuses on the dynamics during this quasi-steady period.

[18] In general, the structure of a river mouth has a significant impact on the near-field plume dynamics (M. Kashiwamura and S. Yoshida, Outflow dynamics at a river mouth, paper presented at 16th Coastal Engineering Conference, American Society of Civil Engineers, Hamburg, Germany, 1978). In the Merrimack River, the mouth is approximately 300 m wide, and defined by two parallel jetties. Wave activity has generated sand spits across the river mouth and a sizable sandy bar just outside the entrance. As a result, it is only approximately 3 m deep over the bar at low tide. These local bathymetric features result in a bottom attached salt front on the seaward edge of the bar during ebb tide, and the related lift-off of the buoyant plume, as it loses contact with the bottom [e.g., *MacDonald and Geyer*, 2005].

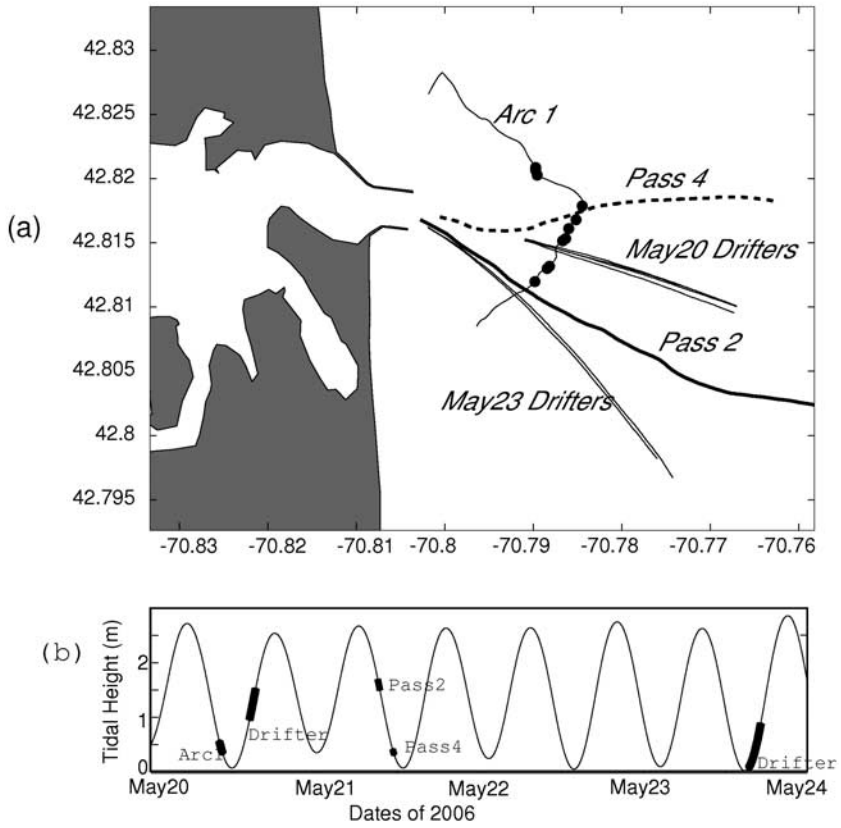

Figure 1. (a) Locations of sampling passes at the mouth of the Merrimack River. Arc 1 is the cross plume section where ship measurements, including CTD and ADCP data, are obtained. Pass 2 and Pass 4 are the two longest passes with results using the control volume approach. The two groups of thinner lines indicate the deployments of surface drifters in 2 days. (b) Time of each of the deployments/passes occurred relative to the tidal stage.

Such a lift-off point only occurs when the river discharge is sufficiently strong to flush the majority of ocean water from the main estuarine channel. In the Merrimack, this occurs during typical freshet conditions, or following large storm events. Near-field salinity contours derived from model output [e.g., *Hetland and MacDonald*, 2008] are shown in Figure 2 for low tide conditions.

2.2. Field Measurements in 2006

[19] The measurements presented in this paper were conducted from 20 May to 23 May 2006, approximately one week after major flooding in the Merrimack River which resulted in a discharge flow of 2700 m^3s^{-1}, the highest in nearly 70 years. Discharges were measured by USGS at station number 01100000 in Lowell, Massachusetts, (approximately 60 km upstream of the mouth). The peak flow was recorded on 15 May 2006, with decreasing flows from 1360 m^3s^{-1} to 1076 m^3s^{-1} recorded during our field operations. The tidal height is approximately 2 meters.

[20] A 1200 kHz Broadband Workhorse acoustic Doppler current profiler (ADCP) (RD Instruments, Inc.) was mounted in a downward looking position off the side of the University of Massachusetts Dartmouth research vessel, the R/V *Lucky Lady*. The ADCP unit sampled at approximately 1 Hz, recorded velocities in 0.25m bins, and it can measure the velocity to a depth of 20 m. An OS200 (Ocean Sensors, Inc.) conductivity, temperature and depth (CTD) profiler, sampling at approximately 6 Hz, was towed by the research vessel, and continuously raised and lowered from the surface to a depth of approximately 4 m. The data set presented in this manuscript includes ADCP and CTD data collected along two passes (Pass 2 and Pass 4 as described by *MacDonald et al.* [2007]) in the along-stream direction and one cross-plume arc, Arc 1, which is approximately 1.2 km away from the river mouth, as shown in Figure 1a. The timing of the passes and deployments with respect to the tidal stage are shown in Figure 1b.

[21] Surface drifters were also deployed to make measurements of currents near the plume surface. The drifters used in this study are a modified version of the drifters described by *Austin and Atkinson* [2004]. The vertical dimension of the drifters was approximately 0.5 m, with less than 10% protruding above the water surface, and a total lateral extent of approximately 1 m. Two drifter deployments were undertaken outside the river mouth during the field experiments. Four drifters were deployed on 20 May, released approximately 1000 m seaward of the mouth at 14:30 local time, which is approximately two hours after low tide. The second drifter release occurred on 23 May, and consisted of two drifters released approximately 200 m outside the river mouth at 15:30 local time, the approximate time of low tide. In both cases, multiple drifters were released simultaneously and

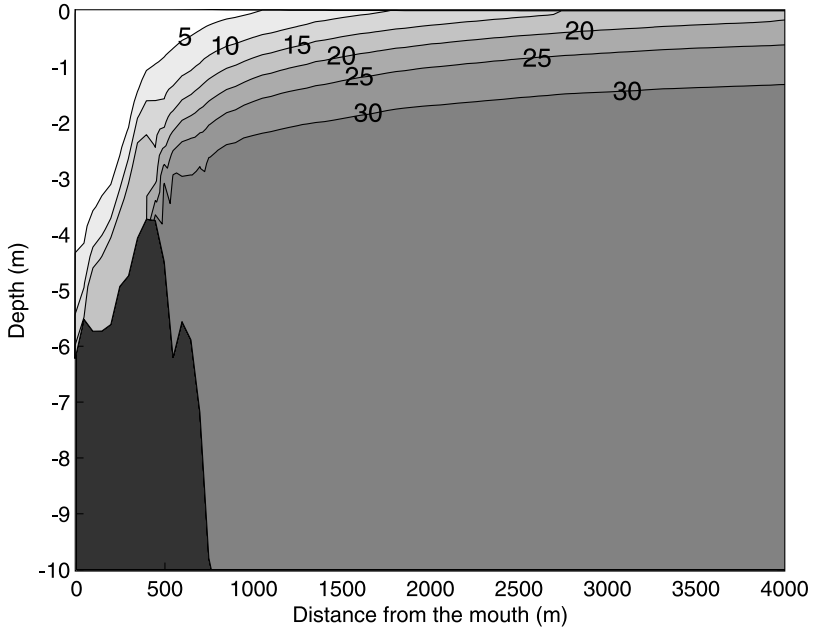

Figure 2. Profiles of salinity through the near-field plume, taken from model output, which shows the lift-off zone over the bar. Seafloor is shown as the dark gray shading.

tracked for about one hour, as shown in Figure 1. The drifters were advected with the surface plume water. It is clear from these drifter tracks that the plume is spreading as it flows away from the estuary mouth.

[22] A numerical model of the Merrimack River plume was developed using the Regional Ocean Modeling System (ROMS). The model set up is same with the one described by *Hetland and MacDonald* [2008]. A curvilinear grid was generated with grid spacing on the order of 10 m near the river mouth. This model considered a steady outflow of 1750 m^3/s to demonstrate the primary results for the time period from late ebb to just past the low tide, as described by *Hetland and MacDonald* [2008]. Model results presented here were taken from one snapshot at six hours after model simulation, providing sufficient time for the model to adjust for the initial conditions. More details of the model set up and results are described by *Hetland and MacDonald* [2008].

3. Measurement Results: Estimates of Plume Spreading

[23] A normalized plume width, defined as W/W_0, is used to examine the local plume spreading rate, where W is the plume width, evaluated here as the standard deviation of drifter positions (for drifter data) or surface streamlines (for model simulation) in the cross plume direction at a given location, with the subscript 0 referring to a reference location. Figure 3 is a schematic map showing the definition of plume width. This parameter, W/W_0, indicates how much the plume spreads laterally compared to the initial point.

[24] For the drifter data, the normalized plume width was estimated as the standard deviation of the cross plume position of all drifters. Although spreading of the plume is not a turbulent process, the use of a standard deviation based width is not unlike the definition of patch size under turbulent diffusion, as described by *Taylor* [1921] in his classic theory of turbulent dispersion. At any given radial distance along the drifter tracks, the standard deviation of the distances between drifters is calculated as W at this distance. The plume width W is then normalized by W_0, which is the plume width at 1000 m seaward from the river mouth. Note that this approach is independent of drifter velocity, as width is evaluated only as the distances between drifter tracks at a given distance from the mouth, and not as the distance between drifters at a specified time. The results from the drifter data are shown in Figure 4. Uncertainty limits are shown for the 20 May drifter

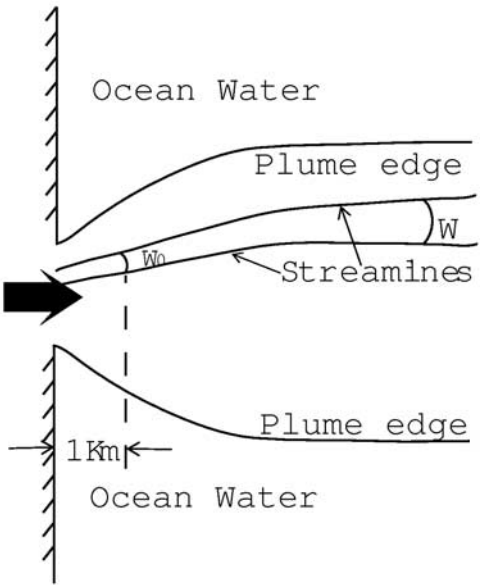

Figure 3. Conceptual sketch of the definition of plume width. The plume width W is the plume width, defined by the distance between streamlines. W_0 is the plume width at 1000 m, considered as the initial plume width value.

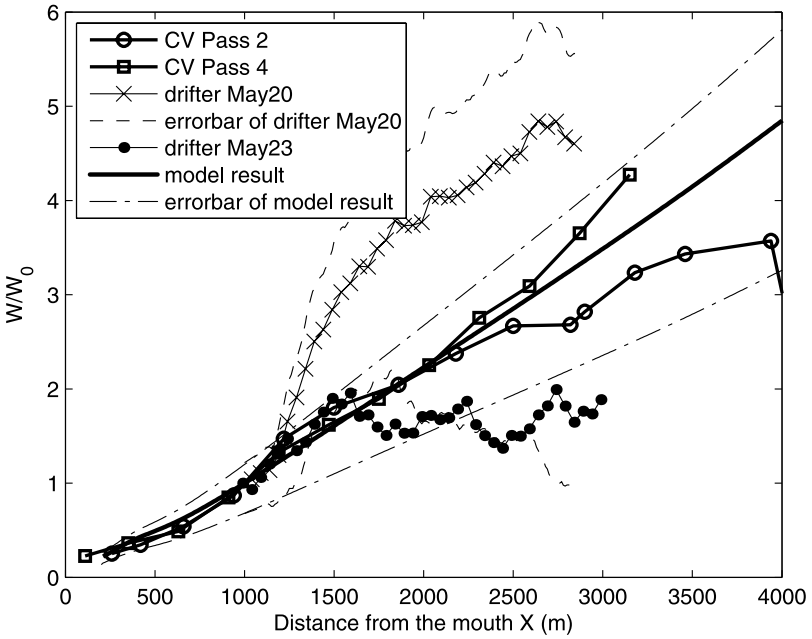

Figure 4. The nondimensional plume width estimated by the control volume method, drifter data, and numerical model. Uncertainty limits of drifter data on 20 May 2006 and model results are shown by the two groups of dash lines.

data, calculated as the minimum and maximum standard deviations associated with the triplet subsets of the four drifters in the deployment. One of the four drifters diverged significantly from the pack during the deployment, resulting in the large uncertainty limits shown in Figure 4, but no cause to remove that drifter from consideration was found. Note that in the study of *Hetland and MacDonald* [2008], approximately 5000 numerical drifters were utilized, yielding statistically robust spreading rates; thus the variability associated with the limited number of drifters in this experiment is not surprising. No uncertainty limits are shown for the 23 May drifter data as only two drifters were deployed on that day. The 23 May deployment does fall within the 20 May uncertainty limits, although the expansion rate for 20 May drifters is higher than that for the 23 May deployment.

[25] The drifter results are compared to the control volume estimates from the two longest sampling transects described by *MacDonald et al.* [2007], as shown in Figure 4 (passes 2 and 4). In general, the drifter results and control volume method demonstrate a similar trend, and all lie within the 20 May drifter uncertainty limits.

[26] The model output from ROMS used here represents the case after six hours of simulation. Figure 5 shows contours of the surface salinity derived from the model snapshot over the region outside the river mouth. The salinity contours indicate that the river plume is deflected slightly to the south outside the mouth. There is no along-shore current imposed on the model domain, so the deflection seen is due primarily to the influence of the earth's rotation.

[27] Figure 6 (top) shows the streamlines defined by the surface flow field from the numerical model. For the streamlines in the top panel of Figure 6, the surface layer is defined as the uppermost portion of the water column responsible for 85% of the integrated fresh water flux in the water column. The streamline patterns again show clearly the trend seen in the salinity contours that the surface plume is deflected to the south rather than spreading radially and symmetrically. The shaded region in the top panel of Figure 6 indicates the plume core (-50° to 15° from due east of the river mouth), defined by *Hetland and MacDonald* [2008] as the relatively homogenous central portion of the flow, which is responsible for the majority of fresh water flux. For this model run, the plume core encompasses 80% of the total fresh water flux observed along the 2 km arc.

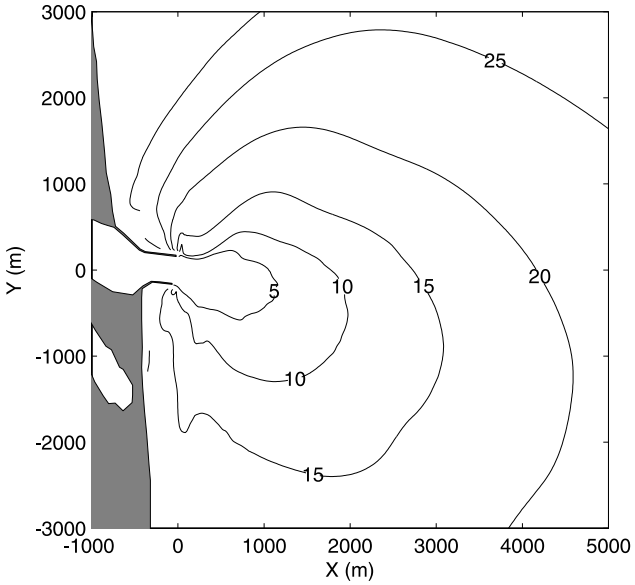

Figure 5. Model results. Contour of surface salinity from one snapshot of the model simulation; *X* and *Y* are distances due east and north from the river mouth.

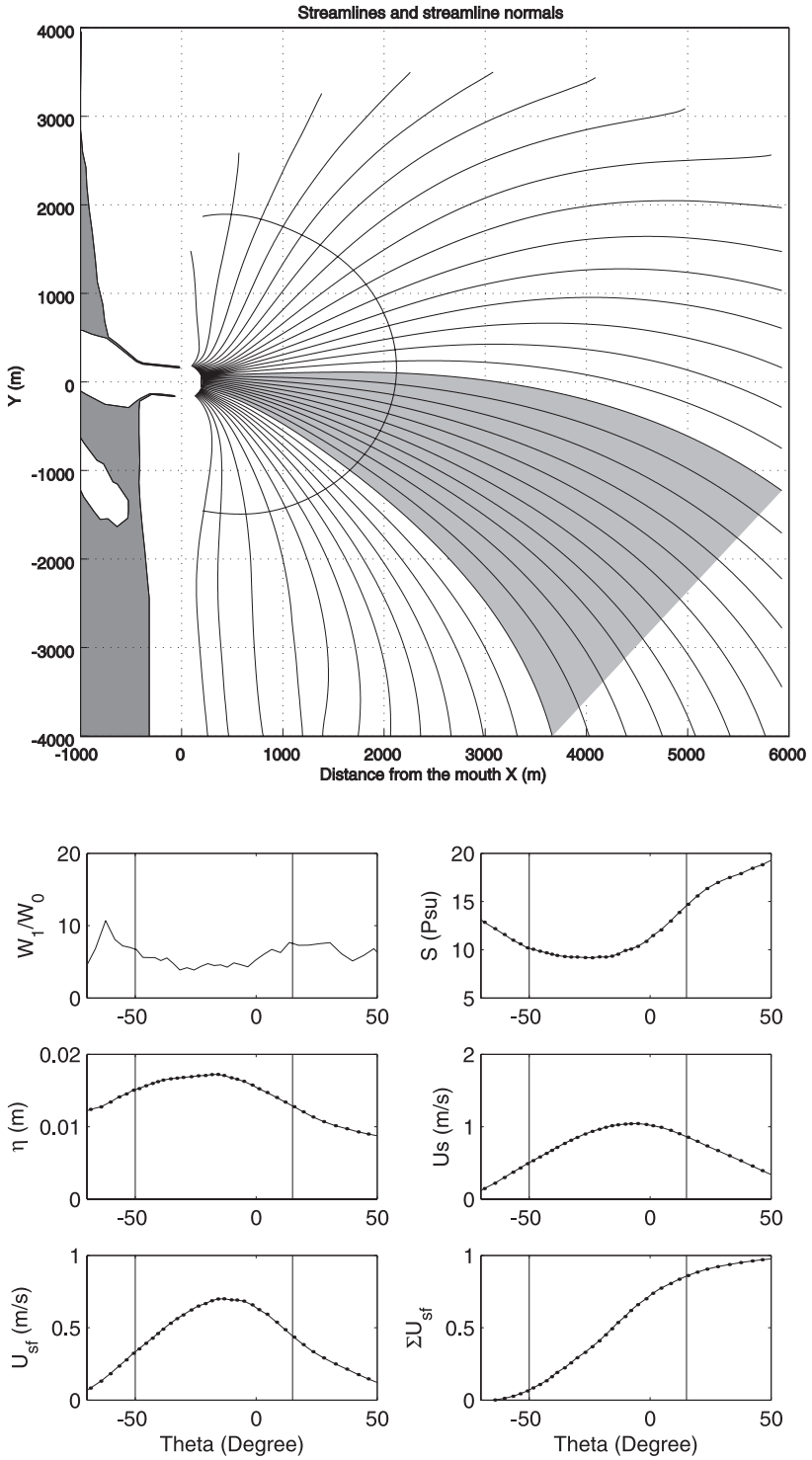

Figure 6. (top) Streamlines from model simulations. The shaded region indicates the plume core. (bottom) Nondimensional plume width (W/W_0), surface salinity (S), surface height (η), surface velocity along streamlines (U_s), fresh water velocity along streamlines (U_{sf}), and the cumulated fresh water velocity along streamlines ($\int\int U_{sf} dz d\theta$). Theta equals to zero at the center of the river mouth and goes counterclockwise direction. Negative theta values represent south side of the estuary. The regions between the two bars in lower panels are the plume core regions.

[28] In the lower panels of Figure 6, specific details along the 2000 m streamline normal are shown, including the local nondimensional plume width (W/W_0), surface salinity (S), surface height (η), streamline velocity (U_s), fresh water streamwise velocity (U_{sf}), equal to the streamwise velocity multiplied by the local "freshness" ($(S_o - S)/S_o$, where S_o is ocean salinity and S is local salinity), and the normalized cumulative fresh water flux ($\int\int U_{sf} dz d\theta$).

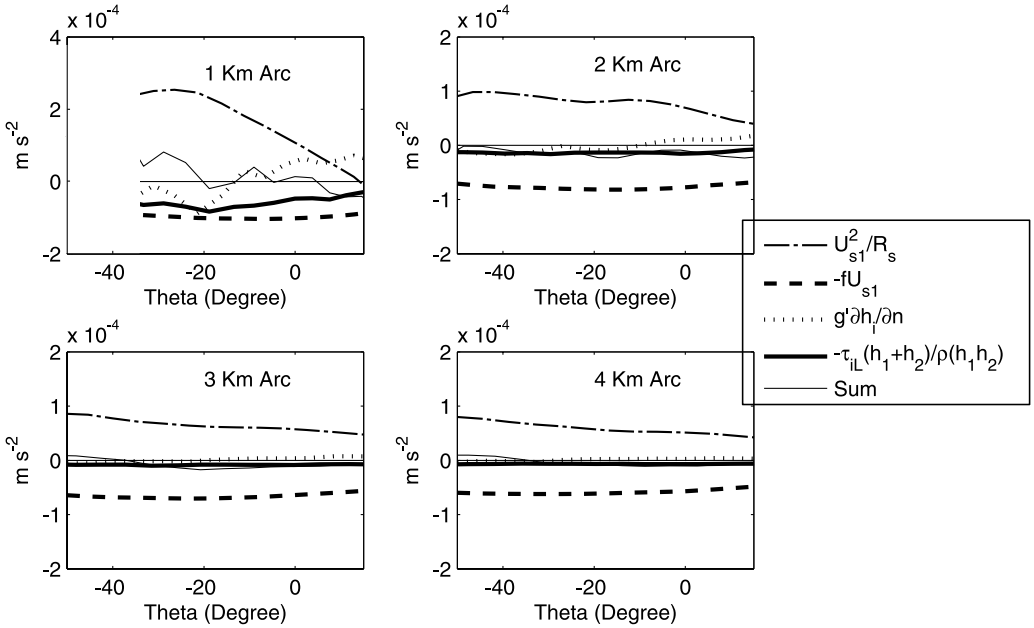

Figure 7. Estimate of terms in the streamline-normal momentum balance (equation (3)) for four arcs from numerical simulation output. The results extend only to −35° at the 1-km arc because of shoreline interaction and local eddy processes that make equation (3) invalid closer to the shoreline.

[29] The normalized spreading widths within the plume core, W/W_0, are also obtained from numerical simulations from 1000 m to 3000 m away from the river mouth, taking the surface streamlines as virtual drifters. These results are plotted along with the field measurements in Figure 4, and they show a reasonable agreement with the drifter data and the control volume results. Uncertainty limits for the model results were generated by taking subsets of all the streamlines used in the estimation. These uncertainty limits are similar in nature to the uncertainty limits associated with the 20 May drifter data, but are tighter to the mean due to the larger number of streamlines (twelve) used in the model calculation as opposed to the four drifters in the 20 May deployment.

[30] In the cross-plume direction, the plume appears to expand faster at the edges (outside the plume core) than within the plume core, shown by the higher W/W_0 value at the edges in Figure 6. This may be considered as the result of stronger barotropic gradients at the plume edges. Also, this trend provides a motivation to examine the lateral momentum balance of the plume, which will be discussed in next section.

4. Discussion

4.1. Lateral Momentum Balance

[31] The lateral momentum balance captures the fundamental processes responsible for plume spreading. Many studies [e.g., *Csanady*, 1975] have shown the importance of the lateral momentum balance for two-layer baroclinic systems, such as coastal jets, estuarine plumes, etc. In the near-field plume, the lateral momentum equation can be reduced to four significant terms as shown in equation (3), and discussed in section 1. The Coriolis term is clearly important for cross-plume dynamics, particularly at larger scales [e.g., *Fong and Geyer*, 2002]. Many studies also show that the curvature and baroclinic pressure gradient in the lateral direction can significantly influence the circulation [*Hench and Luettich*, 2003] and lateral mixing in an estuary [*Alaee et al.*, 2004; *Georgas and Blumberg*, 2004]. Moreover, lateral spreading rate is an indication of the divergence of surface flow streamlines. Thus the rate of change of the local radius of curvature in the streamline normal direction, which is represented by radius of curvature in the centrifugal force term in the momentum equation (3), is directly related to streamline divergence and plume spreading rate.

[32] Analysis of individual terms in the momentum balance provides us insightful information about the mechanisms responsible for lateral spreading. The model output allows estimation of terms in the lateral momentum equation (3). The streamline curvature, R_s, in the first term in equation (3) was directly estimated by fitting a circle to three points taken along the upper layer streamlines of the simulated model flow field. The results of the momentum balance analysis are plotted in Figure 7. At the 1 km arc, the centrifugal force term is balanced by the combined effects of buoyancy, interfacial stress, and Coriolis, while at further arcs, the balance is dominated primarily by Coriolis. Thus in the most energetic portion of the near-field region, spreading is significantly affected by a variety of mechanisms, several of which are directly related to turbulence and mixing. Note that estimates of a corresponding time-dependent term during the late ebb are on the order of 10^{-5} ms^{-2}, confirming that the assumption of steady state during the mid to late ebb is reasonable.

[33] When working with the observational data, equation (3) can be used to obtain estimates of the plume expansion using data from the cross plume transect Arc 1 shown in Figure 1, which has an average distance of 1.2 km away from the river mouth. Values for streamline curvature, R_s, along Arc 1 were estimated from equation (3) by estimating all other terms in equation (3) directly from

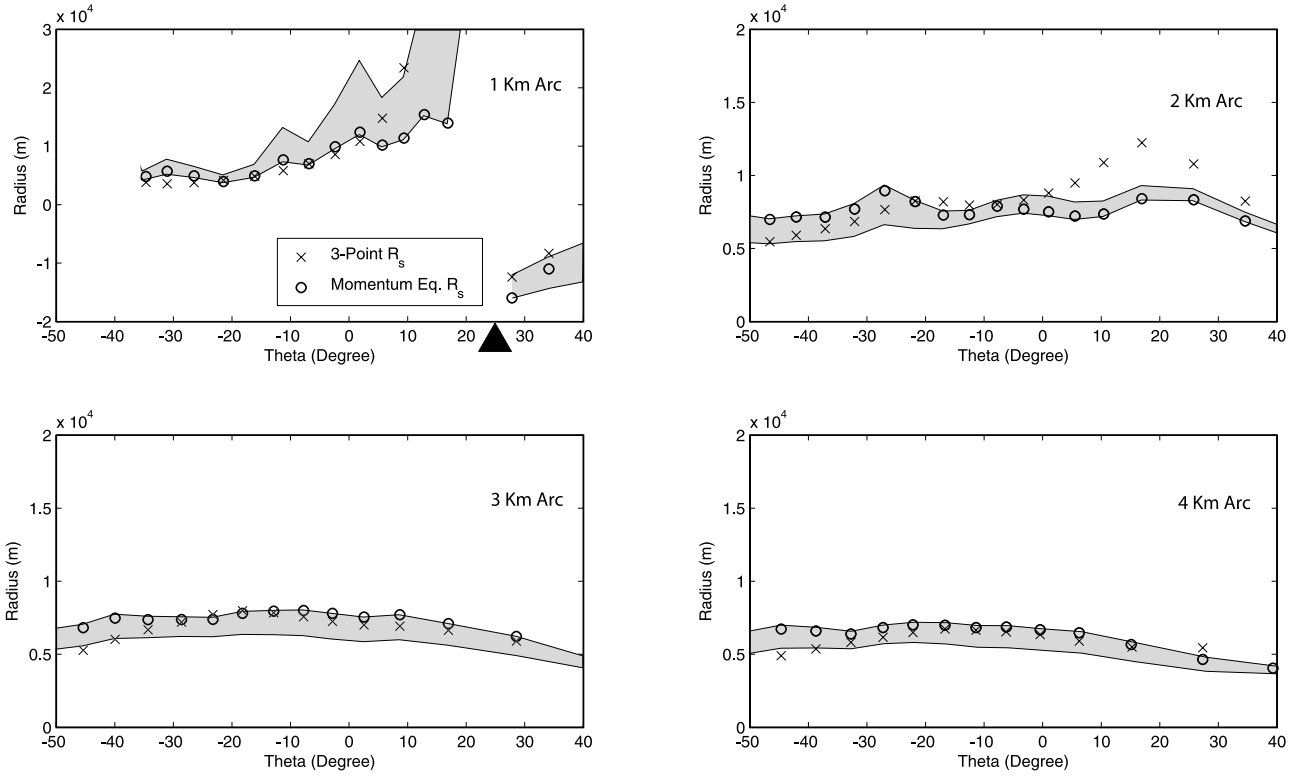

Figure 8. The radius of streamline curvature R_s estimated from a steady state numerical simulation. Cross marks show the results of R_s directly obtained from the upper layer streamlines from model output, using 1000-m interval for the points along streamlines. Black dots are the results using the lateral momentum balance equation (3). The black triangle indicates the centerline of the plume, where the radius of streamline curvature goes to infinity. The shaded areas represent the range of the R_s values derived from equation (3) using the maximum and minimum values of local stress within the limits of the upper layer. The results extend only to -35° at the 1-km arc because of shoreline interaction and local eddy processes that make equation (3) invalid closer to the shoreline.

observational data. Then, lateral spreading rate, represented by normalized plume widths, was evaluated by the divergence of adjacent circles defined by the streamline curvature R_s using a geometric method which will be described in the next section. But first, we will demonstrate that the momentum balance, equation (3), is valid to estimate the radii of streamline curvature using model output.

[34] Using model output, the streamline curvature, R_s, can be estimated with two approaches: the first is described above, fitting a circle to three point from the upper layer streamlines, providing a direct estimate of streamline curvature (we use points separated by 1000 m in the streamwise direction); the second method is substituting model output of velocity and density data into equation (3). Comparison of these two approaches is used here to validate equation (3).

[35] Results of R_s from the two approaches above are shown in Figure 8. Note that for a symmetrically expanding plume without rotation, there is no curvature along the centerline, so that R_s goes to infinity. This is the case in the Merrimack River near-field through the first 1–2 km, until Coriolis forcing begins to curve the entire plume to the south. Limits on the plots in Figure 8 have been set to correspond to the majority of the plume, with the region where R_s goes toward infinity at the 1 km arc shown by the black triangle.

[36] The comparisons of R_s in Figure 8 indicate that the lateral momentum balance suggested by equation (3) works well for the near-field plume region, and can be applied to observational data with some degree of confidence. Most of the lateral spreading in this region is driven by Coriolis force, the pressure gradient due to interface slope, and the lateral interfacial stress due to shear at the layer interface. As distance from the river mouth increases, the Coriolis term increases in importance and the entire plume begins to curve southward.

[37] Given the inherent difficulties associated with dealing with shear layers in a two-layer model, several approaches were taken to evaluating τ_{iL} from model output. The circles shown in Figure 8 were estimated using local stress values taken from the defined layer interface, while the shaded areas in Figure 8 represent the range of the R_s values derived from equation (3) using the maximum and minimum values of local τ_{iL} within the limits of the upper layer. The fact that the envelope defined by the maximum and minimum stress is relatively wider at the 1 km arc than at the further arcs indicates that the interfacial terms are much more important in this region.

4.2. Comparison of Observations to Model Results

[38] Now we can utilize equation (3) to estimate the plume spreading with observational data from Arc 1. Because equation (3) is derived specifically within a streamline coordinate system, only portions of the Arc 1 data were used,

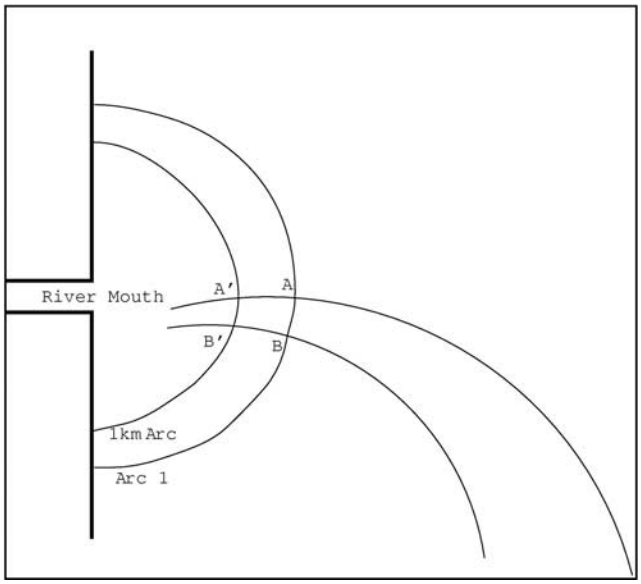

Figure 9. Schematic map of estimation of normalized plume width using observational data along Arc 1 with geometric method. Arc 1 has an average distance of 1.2 km away from the river mouth. *A* and *B* are two adjacent points on Arc 1. A' and B' are intersections of the two circles defined by the local streamline curvature radius and the 1-km arc.

shown by thicker black lines on Arc 1 in Figure 1, where the orientation of the ship track was within ±10° of normal to the locally evaluated direction of the upper layer velocity vectors. The interfacial stress term in equation (3) was evaluated by using locally observed data to determine $\partial u_n/\partial z$, while relying on model output for representative values of the local turbulent eddy diffusivity, which was shown to compare well with observations in *MacDonald et al.* [2007].

[39] The geometric method of plume spreading estimation for Arc 1 is shown by the cartoon in Figure 9. The total spreading rate at any point within the plume is ultimately the superposition of two distinct components; (1) the angular difference between adjacent tangential streamline vectors (e.g., even with no streamline curvature, significant spreading may occur if the otherwise straight streamlines are not parallel to each other), and (2) the curvature imposed on each streamline in the downstream direction (e.g., a positive gradient of the streamline curvature in the streamline-normal direction, is indicative of a divergence of flow in that location, causing the flow to expand laterally as it propagates downstream). The geometric method outlined in Figure 9 naturally accounts for both of these components in identifying the divergence of streamlines across a relatively small distance. Here we follow streamlines from their observed location back to the 1 km arc. Prediction across larger distances is precluded by the potential for changes in the radii of curvature along streamlines. For any two adjacent points A and B on Arc 1, which is approximately 1.2 km away from the river mouth, we can obtain the radius of the streamlines crossing Arc 1 at point A and B using equation (3). We were also able to find the intersection points of the semicircle at 1 km and the two arcs defined by the streamline curvature at A and B. Those two intersection points were shown as A' and B' in Figure 9. The ratio of the arc length between A and B and the arc length between A' and B' is referred to as the normalized plume width at Arc 1.

[40] The approach described above was applied to the observational data at Arc 1. The results from the Arc 1 analysis are shown as the black dots in Figure 10, and compare well with the results from model simulations and other observational data. The limits of Figure 10 represent only a small subset of the wider limits evaluated in Figure 4, due to the limited scales achievable with the method described in Figure 9. It should be noted that inclusion of the stress term appears less significant in the observation driven momentum analysis than in the model, affecting most values of W/W_0 by less than 10%.

[41] The comparisons in both Figure 10 and Figure 4 show similar trends between the estimates, with reasonably good agreement between drifter data, numerical model results and the Arc 1 data within 1 km $\sim$ 2 km region. The agreement from the lateral momentum analysis with the more direct estimates of plume spreading reinforces the conclusion that lateral spreading is well described by equation (3).

[42] Pure radial spreading (i.e., no streamline curvature) was plotted in Figure 10 as a reference line. Most of the results from the Merrimack plume are above this line, which indicates that the plume is spreading faster than pure radial spreading and the plume is divergent, due primarily to streamline curvature. This agrees with the results of *Hetland and MacDonald* [2008], who reached the same conclusion by evaluating the principal strain rate from model output.

[43] A hypothetical normalized plume width based on the local internal gravity wave speed, $c = \sqrt{g'h}$, is also shown in Figure 10, where c was evaluated locally based on model output as described in the introduction. These results represent the lock exchange solution, which agrees well with estimates of lateral spreading from other observational and numerical approaches in the region from 1 km to 2 km, presented in Figure 10. As discussed earlier, spreading consists of a radial component, and a component depending on the local gradient of streamline curvature. At the 1 km arc, the local momentum balance is dominated by four important terms: streamline curvature, Coriolis, interface slope, and interfacial stress. The interface slope term, $-g'\frac{\partial h_i}{\partial n}$, which represents the effect of buoyancy, and is related to the interval wave speed $\sqrt{g'h_i}$, is primarily responsible for observed gradients in streamline curvature. Gradients in curvature related to the Coriolis term are limited, and are directly related to velocity gradients in the cross-plume direction, which are relatively small. Therefore within the first 2 km, the spreading rate is essentially constrained by buoyancy, yielding the good agreement with the lock-exchange solution shown in Figure 10. As the plume propagates further from the mouth, the interface slope term becomes weaker and weaker, thus the Coriolis term becomes increasingly significant. Ultimately, the lateral momentum balance is dominated by only the centrifugal and Coriolis terms.

4.3. Relationship Between Spreading and Mixing

[44] A key reason for studying near-field plumes is the importance of the region in mixing estuarine discharges into the ambient waters of the coastal ocean. Several recent studies [e.g., Hetland, 2005] have suggested that mixing within the small near-field region may be of the same order

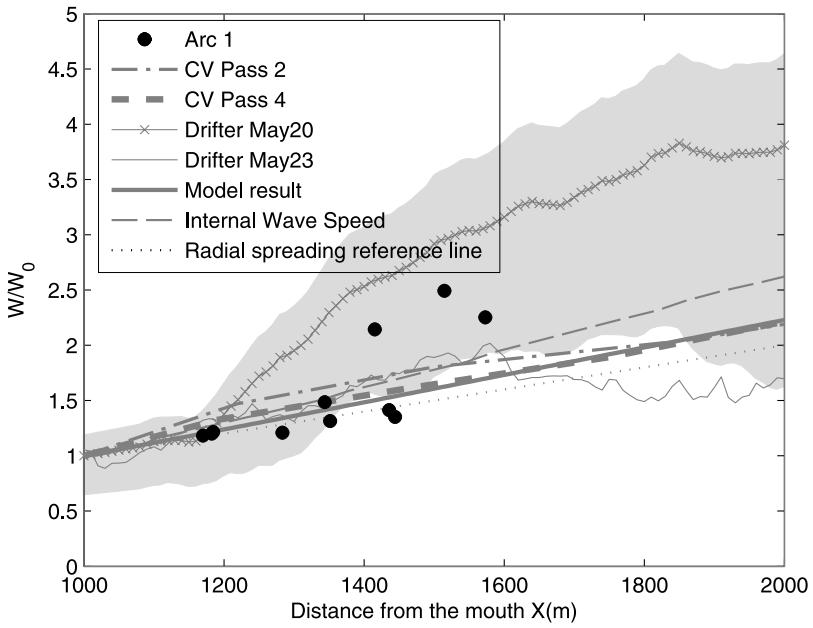

Figure 10. The nondimensional plume widths estimated by observational data along Arc 1 were shown as the black dots, with results from other methods plotted in the same figure. Pure radial expansion width is shown using a thin dash line as reference. Shaded area is the uncertainty limits for 20 May drifter data.

as the total mixing occurring across the much larger far-field plume region. In the near-field region, spreading and mixing are linked in a highly nonlinear and poorly understood manner [e.g., *MacDonald et al.*, 2007; *Hetland*, 2009], and thus an understanding of plume spreading may be essential to developing a more refined understanding and predictive capacity for stratified mixing in the near field region. Here we discuss the significance of the present findings with regards to the spreading-mixing relationship.

[45] Analysis of the lateral momentum balance shows that the interfacial stress term may be important at the 1 km arc, but is less significant at greater distance. The lateral momentum balance is dominated by streamline curvature, buoyancy, Coriolis and interfacial stress at 1 km, but is primarily a balance only between streamline curvature and Coriolis further from the river mouth. To the extent that the lateral forcing mechanisms result in a gradient of streamline curvature across the plume, spreading may be modified from the default condition driven by the seaward propagation of diverging streamlines. In the outer portions of the near-field region, where Coriolis is the primary force balancing curvature, cross-plume gradients in curvature are directly proportional to cross-plume gradients in velocity. In the first 1–2 km, the balance is more complicated, with mixing clearly playing a role in defining the radius of curvature.

[46] These results indicate a potentially complex relationship between spreading and mixing during the early stages of plume evolution. Within the first 1–2 km from the river mouth, mixing between plume and ambient waters influences spreading in two ways. First the local interfacial stress term, driven by turbulence within the shear stratified layer, directly affects the radius of curvature, and thus the spreading rate. Second, the integrated effect of mixing along a streamline reduces the density anomaly between the plume and ambient waters, and adjusts the plume thickness, affecting the local internal gravity wave speed $\sqrt{g'h_i}$, and the buoyancy term in equation (3). Mixing processes also serve to decelerate the plume which can have a significant effect on the spatial representation of plume spreading (i.e., a slower forward propagating plume with the same internal wave speed, will appear to have a larger normalized plume width), by effectively altering the internal Froude number. Deceleration of the plume, particularly different rates of deceleration across the plume, may also play a significant role in the forcing of plume spreading through Coriolis effects.

5. Conclusions

[47] This paper presents estimates of the lateral spreading rate of the near-field Merrimack River plume derived from surface drifter data, numerical model output and cross-plume hydrographic data. The results show reasonable agreement between various methods. The three methods above are valid for the normalized plume width estimates in our study area. The results also agree well with findings in a previous related study [*MacDonald et al.*, 2007].

[48] The spreading rates estimated from our analysis supports the conclusion that the plume spreading rate is related to the local internal gravity wave speed, which is consistent with the theory presented in *Hetland and MacDonald* [2008]. Furthermore, the lateral momentum balance is dominated by streamline curvature, buoyancy, Coriolis, and interfacial stress in the very near-field region (within 1–2 km), but is a balance primarily between streamline curvature and Coriolis further from the mouth.

[49] **Acknowledgments.** This work was funded by National Science Foundation grant OCE-0550096. This manuscript is contribution 09-0501 in the SMAST Contribution Series, School for Marine Science and Technology, University of Massachusetts, Dartmouth. The authors would like to thank L. Rubiano-Gomez, J. O'Hern, and R. Rock for their help with the data collection.

References

Adams, E. E., and K. D. Stolzenbach (1977), Analysis of a buoyant surface discharge over a shallow sloping bottom, in *Proceedings of XVII International Association of Hydraulic Research (IAHR) Congress, Baden, Germany*, pp. 363–370, Int. Assoc. of Hydraul. Res., Madrid, Spain.

Alaee, M. J., I. Greg, and R. Charitha (2004), Secondary circulation induced by flow curvature and Coriolis effects around headlands and islands, *Ocean Dyn.*, *54*(1), 27–38.

Austin, J., and S. Atkinson (2004), The design and testing of small, low-cost GPS-tracked surface drifters, *Estuaries*, *27*, 1026–1029.

Brugge, B. (1995), Near surface mean circulation and kinetic energy in the central North Atlantic from drifter data, *J. Geophys. Res.*, *100*, 20,543–20,554.

Chen, F., and D. G. MacDonald (2006), Role of mixing in the structure and evolution of a buoyant discharge plume, *J. Geophys. Res.*, *111*, C11002, doi:10.1029/2006JC003563.

Csanady, G. T. (1975), Lateral momentum flux in boundary currents, *J. Phys. Oceanogr.*, *5*, 705–717.

Fong, D. A., and W. R. Geyer (2002), The alongshore transport of freshwater in a surface-trapped river plume, *J. Phys. Oceanogr.*, *32*, 957–972.

Garvine, R. W. (1984), Radial spreading of buoyant, surface plumes in coastal waters, *J. Geophys. Res.*, *89*(C2), 1989–1996.

Georgas, N., and A. F. Blumberg (2004), The influence of centrifugal and Coriolis forces on the circulation in a curving estuary, in *Proceedings of the 8th International Conference on Estuarine and Coastal Modeling (ECM8), 3–5 November 2003, Monterey, California*, edited by M. L. Spaulding, pp. 541–558, Am. Soc. of Civ. Eng., Washington, D. C.

Geyer, W. R. (1993), Three-dimensional tidal flow around headlands, *J. Geophys. Res.*, *98*(C1), 955–966.

Hench, J. L., and R. A. Luettich Jr. (2003), Transient tidal circulation and momentum balances at a shallow inlet, *J. Phys. Oceanogr.*, *33*, 913–932.

Hetland, R. D., and D. G. MacDonald (2008), Spreading in the near-field Merrimack River plume, *Ocean Modell.*, *21*, 12–21, doi:10.1016/j.ocemod.2007.11.001.

Hetland, R. D. (2005), Relating river plume structure to vertical mixing, *J. Phys. Oceanogr.*, *35*(9), 1667–1688.

Hetland, R. D. (2009), The effects of mixing and spreading on density in near-field river plumes, *Dyn. Atmos. Oceans*, in press.

Horner-Devine, A. R., D. A. Jay, P. M. Orton, and E. Y. Spahn (2009), A conceptual model of the strongly tidal Columbia River plume, *J. Mar. Syst.*, in press.

Jirka, G. H., E. E. Adams, and K. D. Stolzenbach (1981), Buoyant surface jets, *J. Hydraul. Div., Proc. ASCE*, *107*(HY11), 1467–1487.

Lentz, S. J., and J. Largier (2006), The influence of wind forcing on the Chesapeake Bay buoyant coastal current, *J. Phys. Oceanogr.*, *36*, 1305–1316.

Lentz, S. J., S. Elgar, and R. T. Guza (2003), Observations of the flow field near the nose of a buoyant coastal current, *J. Phys. Oceanogr.*, *33*, 933–943.

Luketina, D. A., and J. Imberger (1987), Characteristics of a surface buoyant jet, *J. Geophys. Res.*, *92*(C5), 5435–5447.

MacDonald, D. G., and W. R. Geyer (2004), Turbulent energy production and entrainment at a highly stratified estuarine front, *J. Geophys. Res.*, *109*, C05004, doi:10.1029/2003JC002094.

MacDonald, D. G., and W. R. Geyer (2005), Hydraulic control of a highly stratified estuarine front, *J. Phys. Oceanogr.*, *35*(3), 374–387.

MacDonald, D. G., L. Goodman, and R. D. Hetland (2007), Turbulent dissipation in a near-field river plume: A comparison of control volume and microstructure observations with a numerical model, *J. Geophys. Res.*, *112*, C07026, doi:10.1029/2006JC004075.

McCabe, R. M., B. M. Hickey, and P. MacCready (2008), Observational estimates of entrainment and vertical salt flux in the interior of a spreading river plume, *J. Geophys. Res.*, *113*, C08027, doi:10.1029/2007JC004361.

O'Donnell, J. (1988), A numerical technique to incorporate frontal boundaries in two-dimensional layer models of ocean dynamics, *J. Phys. Oceanogr.*, *18*, 1584–1600.

Taylor, G. I. (1921), Diffusion by continuous movements, *Proc. Lond. Math. Soc.*, 20,196–20,212.

Wright, L. D., and J. M. Coleman (1971), Effluent expansion and interfacial mixing in the presence of a salt wedge, Mississippi River Delta, *J. Geophys. Res.*, *76*(36), 8649–8661.

Yankovsky, A. E., and D. C. Chapman (1997), A simple theory for the fate of buoyant coastal discharges, *J. Phys. Oceanogr.*, *27*, 1386–1401.

F. Chen and D. G. MacDonald, Department of Estuarine and Ocean Sciences, School for Marine Science and Technology, University of Massachusetts Dartmouth, 200 Mill Road, Suite 325, Fairhaven, MA 02719, USA. (g_fchen@umassd.edu)

R. D. Hetland, Department of Oceanography, Texas A&M University, Room 618D, Oceanography and Meteorology (O&M) Building, College Station, TX 77843-3146, USA.